Article:
Chen, Y, Ye, Q, Jiang, HS et al. (2 more authors) (2019) Conodonts and carbon isotopes during the Permian-Triassic transition on the Napo Platform, South China. Journal of Earth Science, 30 (2). pp. 244-257. ISSN 1674-487X

https://doi.org/10.1007/s12583-018-0884-3

Conodonts and carbon isotopes during the Permian-Triassic transition on the Napo Platform, South China

Yan Chen[a,b], Qian Ye[a,b,d], Haishui Jiang[a,b※], Paul B. Wignall[c], and Jinling Yuan[a,b]

[a]*State Key Laboratory of Biogeology and Environment Geology, China University of Geoscience, Wuhan 430074, China.*

[b]*School of Earth Sciences, China University of Geoscience, Wuhan, 430074, China.*

[c]School of Earth and Environment, University of Leeds, Leeds LS2 9JT, UK.

[d]Non-ferrous Metals Geological Exploration Bureau of Zhejiang Province, Shaoxing, 312000, China

Corresponding author※: jiangliuis@163.com

Yan Chen's ORCID: https://orcid.org/0000-0002-1606-6755

Haishui Jiang's ORCID: https://orcid.org/0000-0001-9636-0307

Abstract

Two Permian–Triassic boundary (PTB) sections (Pojue and Dala) are well exposed in an isolated carbonate platform (the Napo Platform) on the southwestern margin of the Nanpanjiang Basin, South China. These sections provide an insight into the transition across the PTB and a detailed investigation of the conodont biostratigraphy and inorganic carbon isotopes is presented. The PTB at the Pojue Section is placed at the base of Bed 10B (a dolomitized mudstone found below a microbialite horizon), defined by the first occurrence of *Hindeodus parvus*. At the Dala Section, four conodont zones occur. They are, in ascending order, the *Hindeodus parvus* Zone, *Isarcicella staeschei* Zone, *Isarcicella isarcica* Zone and *Clarkina planata* Zone. Comparison with the Pojue Section suggests the PTB at Dala also occurs at the base of dolomitized mudstone below a microbialite horizon, although the first occurrence

of *Hindeodus parvus* is towards the top of a microbialite bed: an occurrence that is also seen in other platform sections. The succeeding microbialite beds developed during the ongoing PTB mass extinction phase. This time was characterized by low carbon isotope values, and a microbialite ecosystem that provided a refuge for select groups (bivalves, ostracods and microgastropods) that were likely tolerant of extremely high temperatures.

Key words: Permian-Triassic; Napo Platform; conodont biostratigraphy; carbon isotope

1. Introduction

The largest mass extinction in geological history occurred around the Permian-Triassic boundary (PTB). It has been studied for several decades and various extinction patterns (e.g., Shen et al., 2018, 2011; Jiang et al., 2015; Wignall, 2015; Wang et al., 2014; Song et al., 2013; Yin et al., 2012) noted with numerous causes (e.g., Sun et al., 2018; Baresel et al., 2017; Ernst and Youbi, 2017; Foster et al., 2017; Brand et al., 2016; Chen B et al., 2016; Grasby et al., 2016; Xiang et al., 2016; Chen Z-Q et al., 2015; Clarkson et al., 2015; Jiang et al., 2015; Song et al., 2014; Yin et al., 2014; Joachimski et al., 2012; Sun et al., 2012) proposed, but debate on the timing and nature of the crisis continues. Much of this discussion has been focused on sections in South China, notably the Global Stratotype Section and Point (GSSP) at Meishan and the auxiliary GSSP at Shangsi. Many sections in the Nanpanjiang Basin area have also provided important insights into PTB events, e.g., the persistence of siliceous deposition into the Early Triassic at Gaimao (Yang et al., 2012), the occurrence of delayed extinction in the deep-

water location of Bianyang (Jiang et al., 2015) and the age of post-extinction microbialite facies following a hiatus in shallow, carbonate settings (Baresel et al., 2017; Jiang et al., 2014) at the Great Bank of Guizhou (GBG).

Like the GBG, the Napo Platform is also found within the Nanpanjiang Basin, being located near the southwestern margin (Fig. 1). We have undertaken the first study of conodont biostratigraphy and $\delta^{13}C_{carb}$ fluctuations at the Pojue and Dala sections (Fig. 1), in order to better constrain the mass extinction and environmental changes during the PTB on this little studied Platform.

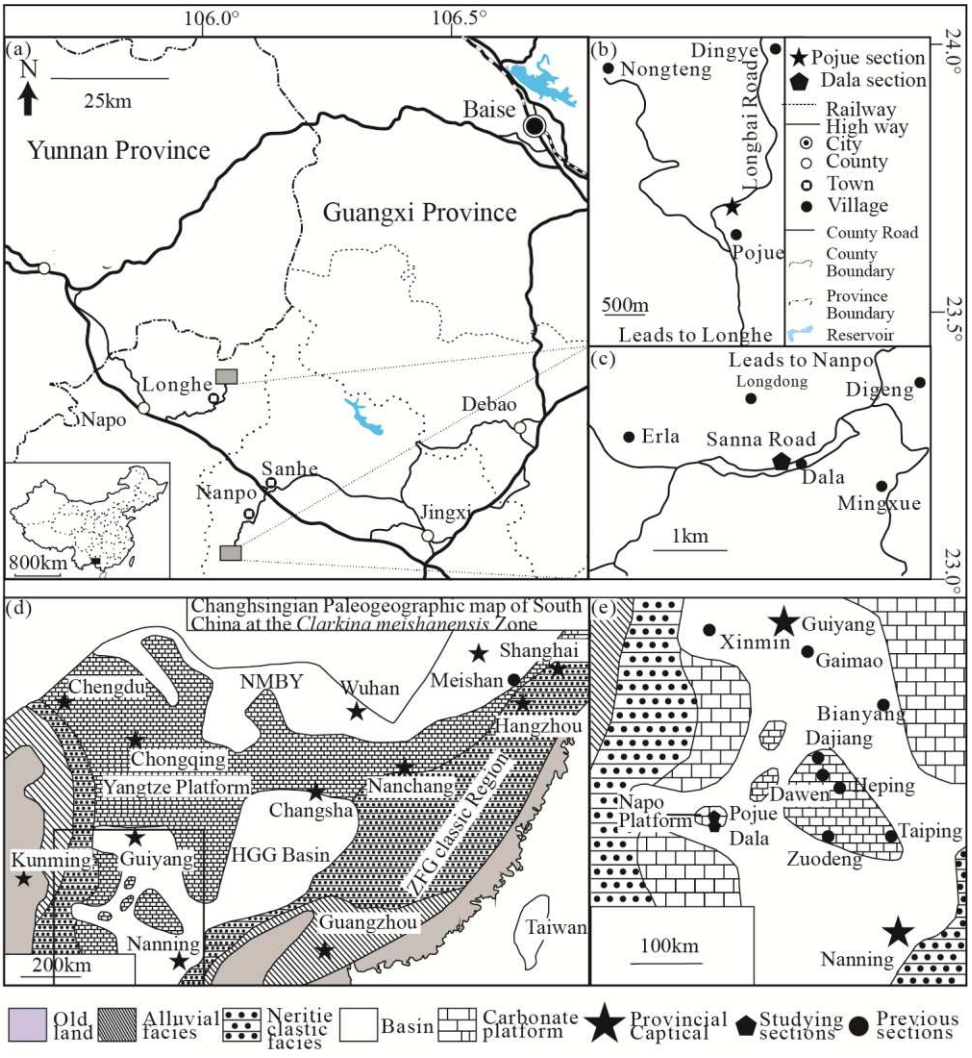

Figure. 1 Location of the study sections and Changhsingian paleogeographic map of South China during the latest Permian *Clarkina meishanensis* Zone. Revised after Yin et al. (2014), NMBY, North marginal basin of Yangtze Platform; HGG Basin, Hunan–Guizhou–Guangxi basin; ZFG clastic Region, Zhejiang–Fujian–Guangdong clastic Region.

2. Geological settings and facies description

The Pojue Section is located at Pojue village, Longhe town, Napo County (Fig. 1). The Dala section occurs about 37 km south of Pojue and is located at Dala village, Nanpo town, Jingxi County (Fig. 1). These two sections record carbonate-dominated marine sedimentation during the PTB interval and are well exposed and easily accessible.

The Upper Permian strata at Pojue are dominated by bioclastic packstone and algal-laminated bindstone of the Wuchiaping Formation. The former lithology has a rich biota that includes fusulinids, foraminifers, calcareous algae and ostracods (Fig. 2 a). Only calcareous algae and foraminifers occur in the algal-laminated bindstone. The diverse biota indicates an open shallow-marine setting and a low to moderately high-energy environment in the Late Permian.

The Permian-Triassic transition strata of Pojue consist of an 8 cm-thick limestone bed (Fig. 2 a), which occurs above the algal-laminated bindstone and is overlain by microbialite. It consists of dolomitized mudstone (Bed 10B, Fig. 2d), foraminiferal cortoid grainstone (Bed 10A, Fig. 2d) and stromatolites with wavy laminae. These lithologies occur as multiple distinct units bounded by uneven or irregular truncation

surface shown in Fig. 2b. The lowest Triassic bed is a dolomitized mudstone that only yields *H. parvus*. It is bounded by truncation surfaces and is overlain by microbialite (Fig. 2b). The dolomite crystals are dirty with inclusions (Fig. 2d, Bed 10B).

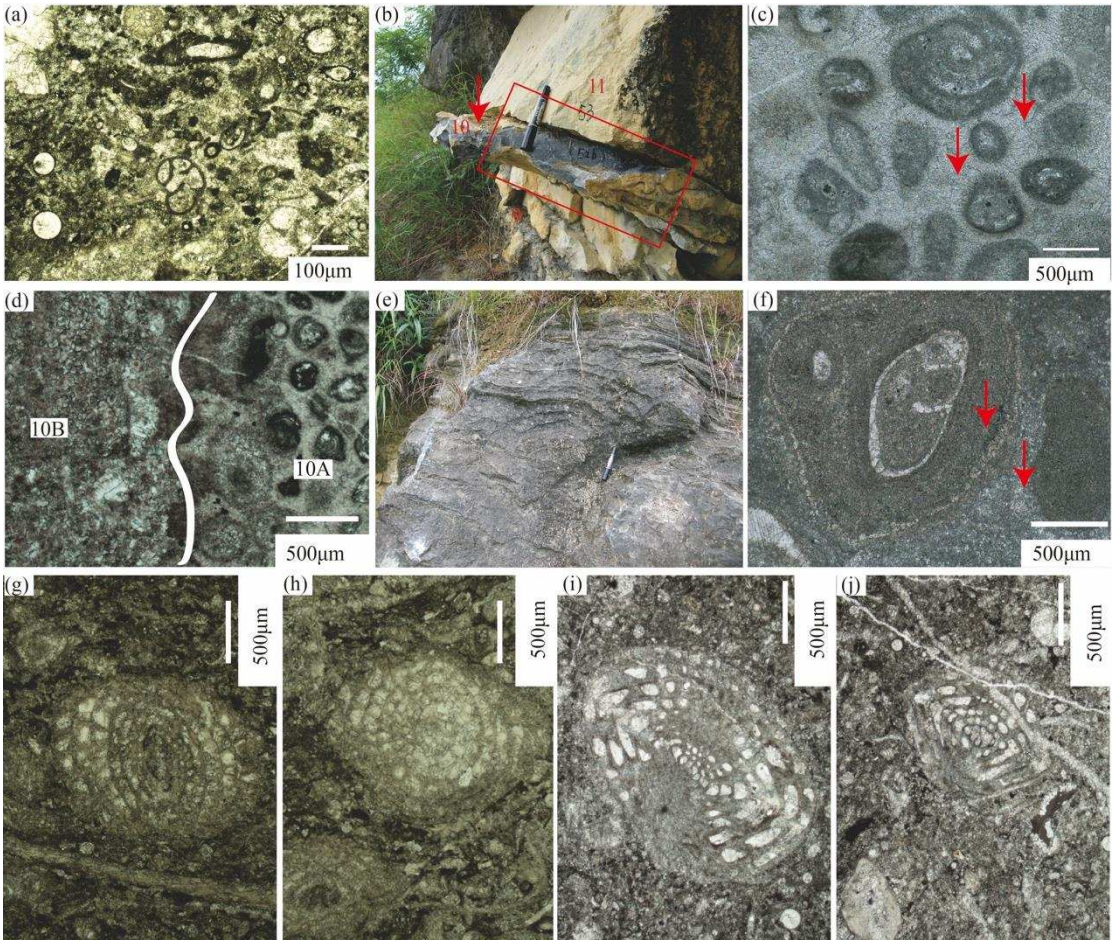

Figure. 2 Outcrop and thin section photographs of Permian-Triassic Boundary strata at the Pojue section and foraminifer at the Pojue and Dala sections. (**a**): Bioclastic packstone at Pojue, Bed 1; (**b**): Outcrop view of PTB at the Pojue section, red arrow shows the dolomitized mudstone, a 0.15m marker pen provides scale; (**c**): The cortoid grainstone of Bed 10A at Pojue, the red arrows show isopachous fibrous rims around micrite envelopes; (**d**): Thin section photo of the uneven surface (vertical in this view) between the Beds 10B and 10A at Pojue; (**e**): Outcrop photo of calcimicrobial framestone with microbialite mound at Pojue, Bed 12, a 0.15m maker pen provides scale; (**f**): Thin section photo of an ooid in Bed 13 at Dala. The red arrows show both sides of the ooid have same

89 characteristic and its inconspicuous laminate; (**g**)-(**j**): fusulinids at the Pojue and Dala sections, (**g**), (**i**), (**j**):
90 *Nankinella* sp.; (**h**): *Pisoina* sp.; (**g**), (**h**): 2.76m below the base of Bed 10 B at Pojue; (**i**), (**j**): from Bed 7 at Dala.

91 Lower Triassic limestones sit on a truncation surface (Fig. 2 e) at the top of the
92 dolomitized mudstone (Bed 10B) mentioned above or stromatolites (Bed 10C) of the
93 Permian-Triassic transition Bed. The 6 m-thick, calcimicrobial framestone is composed
94 of thrombolites (characterized by clotted structures), showing occasional domal
95 structures (Fig. 2 e). This is in turn overlain by thin-bedded micritic mudstone with
96 ostracods and conodonts. Horizontal bioturbation and thin-shelled fossils are seen in
97 other earliest Triassic thin-bedded strata around this level (e.g. Zhao et al., 2008; Baud
98 et al., 2007; Wignall and Hallam, 1996) but these features are absent from the Pojue
99 strata.

100 The lithology of the Dala Section is similar to that of the Pojue Section, but with
101 some minor differences. The upper Permian Wuchiaping Formation bioclastic
102 packstone contain fusulinids, foraminifers, calcareous algae, ostracods and
103 echinoderms, but the absence of algal-laminated bindstone suggests a slightly deeper
104 water setting. The Wuchiaping Formation is once again capped by a truncation surface.
105 Thus, the Dala section consists, in ascending order, of cortoid grainstone with fusulinids
106 and foraminifers, dolomitized mudstone with the conodont *H. praeparvus*, a
107 stromatolite bed and thrombolites. The thrombolites bed in turn is overlain by thin-
108 bedded micritic mudstones that contain ostracods or some thin-shelled fossils. Thin
109 oolitic wackstone beds, 5 cm-10 cm thick, are interleaved with the mudstones. The
110 ooids, 1-2 mm in diameter, are partly recrystallized (Fig. 2 f), although some show more

than one nucleus and a thick cortex with irregular overlapping micritic laminae reminiscent of oncoids (Fig. 2 f). Ooids also occur in GBG sections but as thicker beds of oolitic grainstone (e.g. Li et al., 2015; Tian et al., 2015; Li et al., 2013; Lehrmann et al., 2012). The co-occurrence of ooids, typically produced in agitated conditions and micrite, suggesting quiet energy, at Dala implies the ooids may have formed in shallower waters and then been transported into the depositional setting.

3. Materials and methods

In order to investigate the conodont biostratigraphy, 17 samples (each > 4 kg in weight) were collected from the Pojue section and 21 samples (each > 4 kg) were collected from the Dala section (Figs. 3 and 5). All samples were broken into fragments then dissolved in dilute acetic acid (10%) and a 2.80 - 2.82 g/ml heavy liquid solution (solution of lithium heteropolytungstates in water) was used to separate the conodonts from the residues (method see to Yuan et al. 2015). In total 2 626 conodont elements belonging to *Hindeodus*, *Isarcicella* and *Clarkina* were obtained. Among them were 29 well preserved P_1 elements from Pojue and 322 well-preserved P_1 elements from Dala (Fig. 3). These materials (Plate. 1-4) enabled the biostratigraphy of the two sections to be evaluated.

Sections	Beds No	Samples No	Lithologic informations	*H. parvus*	*H.*cf. *parvus*	*H. praeparvus*	*H. inflatus*	*H. peculiaris*	*I. inflata*	*I. staeschei*	*I.isarcica*	*I. prisca*	*I. turgida*	*C. carinata*	*C. lehrmanni*	*C. taylorae*	*C. planata*
Pojue	10b	PJC-09	DM	3	3	6											
	10c	PJC-10	DM	2	2	3											
	13	PJC-14	TBM	2		2											
	13	PJC-15	TBM	1													
	13	PJC-16	TBM	2		3											
Dala	9	DAL-2B	DM			3											
	10	DAL-6	CF		1	2											
	11	DAL-11	CF	2		2											
	11	DAL-12	CF	3		2				1			1				
	12	DAL-13	TBM	14		13		5		26	1						
	15	DAL-14	TBM	24		14			4	11							
	17	DAL-15	TBM	50		66	3	11				8	11	1	2	1	1
	17	DAL-16	TBM	9		14											
	17	DAL-17	TBM	2		3							3				
	17	DAL-18	TBM	1		2						2					
	17	DAL-19	TBM	1													

Figure. 3 Numerical distribution of conodont species at Dala and Pojue Sections, Napo and Jingxi County, Guangxi Province. Abbreviations of the genus of conodont and lithologic information: *H., Hindeodus, C., Clarkina, I., Isarcicella*, P1 conodont element, DM, dolomitized mudstone; TBM, thin-bedded mudstone; CF, calcimicrobial framestone.

Both the Pojue and the Dala sections of the Napo Platform in Guangxi Province have been sampled for carbon and oxygen stable isotope investigation. Bulk rock carbonates were sampled by micro drill to produce 2 – 4 mg powders and $^{13}C/^{12}C$ and $^{18}O/^{16}O$ ratios of CO_2 were generated by the acid reaction and measurement on a Finnigan MAT-253 at the State Key Laboratory of Biogeology and Environment Geology in Wuhan and converted to $\delta^{13}C_{carb}$ (VPDB) and $\delta^{18}O$ (VPDB) (Fig. 4).

Samples No.	$\delta^{13}C$ (‰) VPDB	$\delta^{18}O$ (‰) VPDB	Samples No.	$\delta^{13}C$ (‰) VPDB	$\delta^{18}O$ (‰) VPDB	Samples No.	$\delta^{13}C$ (‰) VPDB	$\delta^{18}O$ (‰) VPDB
Pojue			PJ15-12	0.15	-8.40	DALS-6	4.04	-5.96
PJ-1	4.95	-7.37	PJ15-13	0.20	-8.11	DALS-7	3.29	-8.42
PJ-2	4.68	-6.61	PJ15-15	-0.52	-9.10	DALS-8	1.01	-7.77
PJ-3	3.14	-8.28	PJ15-17	-0.33	-7.44	DALS-10	3.95	-6.65
PJ-4	4.87	-5.83	PJ15-19	-0.04	-6.37	DALS-11	4.10	-7.25
PJ-5	5.10	-9.29	PJ15-22	-0.45	-7.39	DALS-12	1.06	-5.64
PJ-6	4.52	-7.38	PJ15-24	-0.42	-7.65	DALS-13	0.51	-5.58
PJ-7	4.74	-6.84	PJ15-26	-0.44	-6.77	DALS-14	0.20	-5.68
PJ-8	5.10	-8.21	PJ15-28	-0.29	-6.75	DALS-15	0.03	-5.29
PJ-12	4.49	-6.69	PJ-24	-0.03	-6.08	DALS-16	-0.32	-5.62
PJ-13	2.97	-6.65	PJ15-30	-0.56	-8.19	DALS-17	-0.01	-4.98
PJ-14	3.19	-5.76	PJ15-32	-0.53	-6.51	DALS-18	0.34	-4.95
PJ-15	3.19	-7.37	PJS-1	1.77	-6.81	DALS-19	-0.39	-5.52
PJ-18	2.98	-6.51	PJS-2	2.06	-7.01	DALS-20	-0.34	-6.19
PJ-19	2.98	-5.50	PJS-3	1.96	-6.15	DALS-21	-0.54	-5.33
PJ-20	1.75	-5.91	PJS-4	1.93	-6.69	DALS-22	0.00	-6.75
PJ15-1	1.42	-6.98	PJS-5	1.91	-5.99	DALS-23	0.13	-5.9
PJ15-2	1.73	-6.09	PJS-6	2.00	-5.44	DALS-24	-0.19	-7.35
PJ-21	0.05	-8.40	PJS-7	2.16	-5.98	DALS-26	-0.23	-6.3
PJ15-3	2.24	-3.08	Dala			DALS-27	1.03	-5.59
PJ15-4	1.72	-5.98	DALS-1	4.04	-8.45	DALS-28	1.23	-6.49
PJ15-6	0.96	-6.13	DALS-2	3.35	-6.94	DALS-29	1.38	-5.49
PJ15-8	-0.09	-7.92	DALS-3	3.48	-5.35	DALS-30	1.19	-5.71
PJ15-10	-1.02	-7.70	DALS-4	3.48	-5.3	DALS-31	1.67	-7.3
PJ-23	-0.41	-7.12	DALS-5	3.76	-6.1			

Figure. 4 Carbon and oxygen ratios of carbonate from Pojue and Dala section, analyzed using MAT 253 in State Key Laboratory of Biogeology and Environmental Geology (China).

4. Results

4.1 Conodont biostratigraphy

4.1.1 The Pojue Section

We failed to obtain any conodonts from Bed 1 to Bed 10A in our collections. However, abundant fusulinids and foraminifera are seen in thin section such as the

147 fusulinids Nankinella sp. and Pisoina sp. (Fig. 2 g and h). In addition, the fusulinids,
148 Sphaerulina and the coral Liangshanophyllum have also been reported from these beds
149 at Pojue, and Palaeofusulina and Codonofusiella are known from the same level
150 regionally and indicate a Late Permian (Changhsingian) age (Regional Geological
151 Survey Team of the Guangxi Zhuang Autonomous Region Geological Bureau, 1974).
152 Two species, *Hindeodus parvus* and *Hindeodus praeparvus* are found at Bed 10B
153 (Fig. 5 and Plate. 1). Although this is not enough to precisely identify a conodont zone,
154 *H. parvus* marks the base of Triassic (Yin et al., 2001), and therefore the beds above
155 Bed 10B, including the microbialite bed, at Pojue can be assigned an Early Triassic
156 (Griesbachian) age.

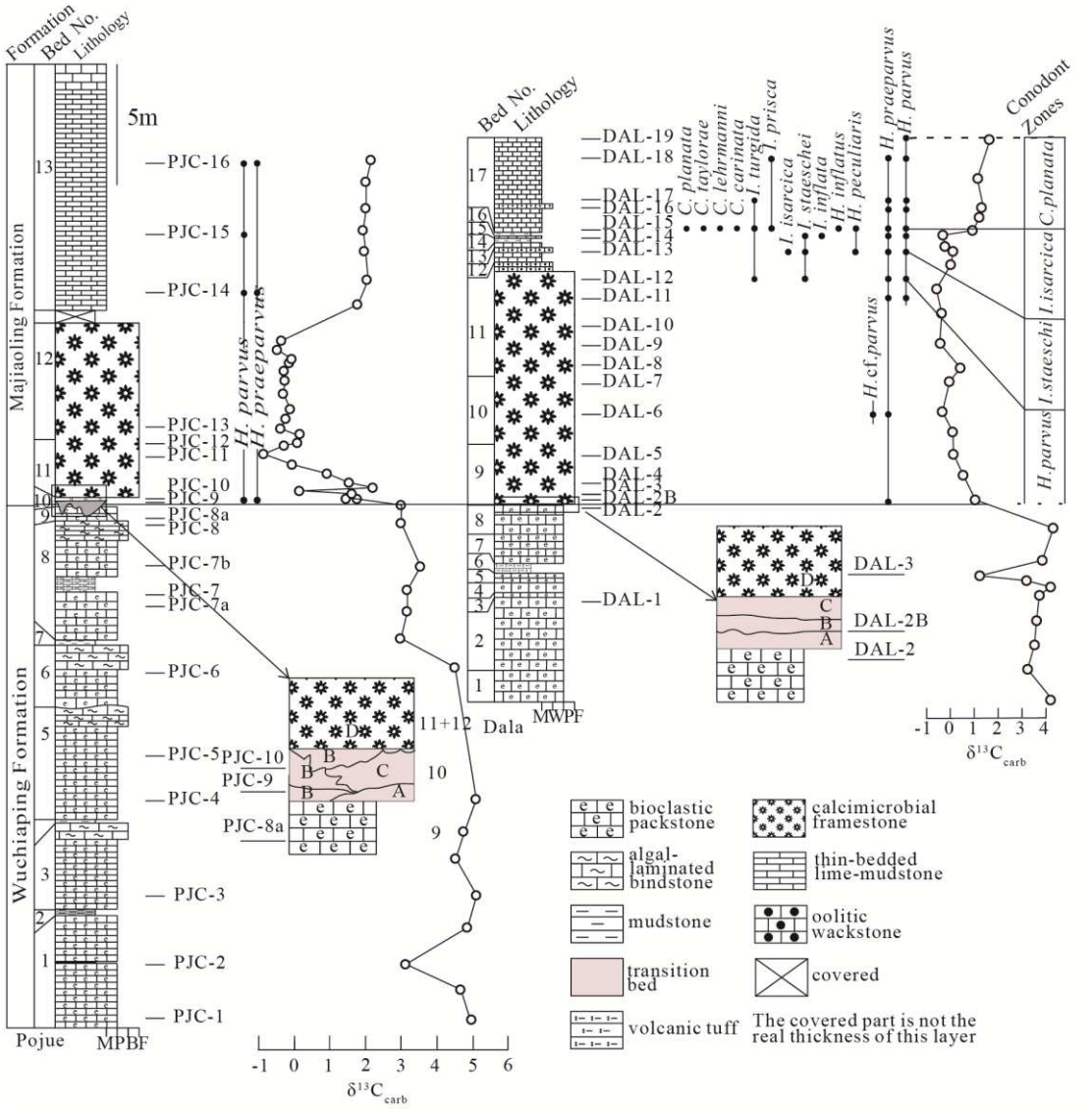

Figure. 5 Lithostratigraphic logs, conodont distributions and carbon isotopes at the Pojue and Dala PTB sections. The arrows show sketch illusions of interpreted contact relationship at transition strata from Permian bioclastic packstone to Triassic microbialite at Pojue and Dala sections. A: cortoid grainstone with foraminifer; B: dolomitized mudstone; C: calcimicrobial framestone with stromatolite; D: calcimicrobial framestone with thrombolite. Abbreviations of the genus of conodont: *H. Hindeodus, C. Clarkina, I. Isarcicella.*

4.1.2 The Dala Section

Beds 1-8 also failed to yield conodonts at the Dala Section. However, the lithostratigraphy of this interval is very similar to that at Pojue and so we also assign a

latest Permian age to these strata at Dala. The lithostratigraphic succession from the base of Bed 9 is the almost same as that from Bed 10 A to C to Bed 11 at Pojue. Fortunately, more conodonts were collected from Bed 9 - 17 at the Dala section, enabling the identification of four conodont zones (Plate. 1-4). In ascending order, they are: Hindeodus parvus Zone, *Isarcicella staeschei* Zone, *Isarcicella isarcica* Zone and *Clarkina planata* Zone.

Hindeodus parvus Zone: *Hindeodus parvus* first occurred in sample DAL-11 (Fig. 5). While a specimen of *Hindeodus* cf. *parvus* is found from Bed 10 and *Hindeodus praeparvus* is found from the base of Bed 9 (Fig. 5), based on comparison with the Pojue section, *H. parvus* could appear in base of Bed 9 (Fig. 5) at Dala. Thus, we tentatively place the lower limit of this zone at the base of Bed 9. The upper limit is defined by the first occurrence of *Isarcicella staeschei*. Associated taxa include *Hindeodus praeparvus* and *Hindeodus* cf. *parvus*. This zone is widely reported in Nanpanjiang Basin area (e.g. Bianyang (Yan et al., 2013), Dajiang (Jiang et al., 2014), Xinmin (Zhang et al., 2014), Dawen (Chen et al., 2009; Liu et al., 2007) and Langpai (Ezaki et al., 2008)).

Isarcicella staeschei Zone: Lower limit: first occurrence of Isarcicella staeschei; upper limit: first occurrence of Isarcicella isarcica. This zone ranges from the base of sample DAL-12 to the base of sample DAL-13 (Fig. 5). Associated taxa: Hindeodus parvus, Hindeodus praeparvus and Isarcicella turgida. The I. staeschei Zone also has been widely reported in Nanpanjiang Basin (e.g. Dawen (Chen et al., 2009; Liu et al.,

187 2007), Langpai (Ezaki et al., 2008) and Heping (Krull et al., 2004; Lehrmann et al.,
188 2003)).

189 Isarcicella isarcica Zone: Lower limit: first occurrence of Isarcicella isarcica; upper
190 limit: first occurrence of Clarkina planata. Associated taxa: H. parvus, H. praeparvus,
191 H. peculiaris, I. staeschei, I. inflata and I. turgida. This zone ranges from the base of
192 sample DAL-13 to the base of sample DAL-15 in the Dala section (Fig. 5). The zone is
193 widely reported from the Nanpanjiang Basin (e.g. Langpai (Ezaki et al., 2008), Dawen
194 (Chen et al., 2009; Liu et al., 2007), Gaimao (Yang et al., 2012) and Dajiang (Jiang et
195 al., 2014)).

196 Clarkina planata Zone: Lower limit: first occurrence of Clarkina planata. The upper
197 limit is undefined. Associated taxa: H. parvus, H. praeparvus, H. peculiaris, I. inflatus,
198 I. prisca, I. turgida, C. lehrmanni, C. carinata and C. taylorae. This zone starts from
199 the base of sample DAL-15 (Fig. 5). Wang (1996) first established the Clarkina planata
200 Zone at Meishan, where it occurs in deep-water facies, and considered that it could
201 correspond to the upper Isarcicella staeschei to Hindeodus postparvus zones in
202 shallower water sections. Zhang et al. (2009) defined a Clarkina tulongensis - Clarkina
203 planata assemblage zone, based on the disappearance of I. isarcica and the first
204 occurrence of Sweetospathodus kummeli from Bed 52-Bed 72 at Meishan. Yang et al.
205 (2012) also reported Clarkina planata Zone at Gaimao in the Nanpanjiang Basin and
206 defined the first occurrence of Clarkina planata and Clarkina krystyni as its base and
207 top, respectively. The Clarkina planata Zone at the Dala section is equivalent to that at
208 Gaimao (Yang et al., 2012).

These four conodonts zones of the Napo Platform can be readily correlated with sections in the Nanpanjiang Basin area and also with the GSSP at Meishan (Fig. 6).

System	Stages	Meishan	Nanpanjiang Basin area			
		Chen Z-Q et al. 2015 (After Jiang et al., 2011,2007; Zhang et al., 2009)	Dawen Chen J et al. (2009); Liu et al. (2007)	Gaimao Yang et al. (2012)	Dajiang Jiang et al. (2014)	Napo platform This paper
Early Triassic	Induan	*Nc. discreta*		*Ns. dieneri*		
				C. krystyni		
		C. planata		*C. planata*	*H. sosioensis*	*C. planata*
		I. isarcica	*I. isarcica*	*I. isarcica*	*I. isarcica*	*I. isarcica*
		I. staeschei	*I. staeschei*			*I. staeschei*
		H. parvus	*H. parvus*		*I. lobata*	*H. parvus*
					H. parvus	
Late Permian	Chanhsingian	*C. taylorae*				
		H. changxingensis				
		C. meishanensis				

Figure. 6 Correlation of the Permian-Triassic conodont zones in selected sections from South China. Abbreviations of the genus of conodont: *H. Hindeodus, C. Clarkina, I. Isarcicella, Nc. Neoclarkina, Ns. Neospathodus.*

4.2 Carbon isotopes

The oldest $\delta^{13}C_{carb}$ values are around +5 ‰ at the base of the Pojue section and decline to +3 ‰ in the uppermost 5 m of the Upper Permian strata. Within the lowest Triassic microbialite bed $\delta^{13}C_{carb}$ values decline rapidly and then reach stable values between –1 ‰ to 0 ‰ in Bed 11 and Bed 12. From Bed 13 upwards the $\delta^{13}C_{carb}$ values recover to higher values around +2 ‰ (Fig. 5).

The $\delta^{13}C_{carb}$ values at Dala show a very similar trend to the Pojue section. Beginning around +4 ‰ in the Upper Permian of the Dala section these values remain stable,

except for two lower values around 2 m from the top, before a rapid shift to light values that range from –0.5 ‰ to 0 ‰ in the microbialite bed (Bed 9 to 16). From the base of Bed 17, the $\delta^{13}C_{carb}$ values return to higher values (around +1 ‰) again (Fig. 5).

5. Discussion

5.1 The Permian-Triassic Boundary

Defined by the first occurrence of *H. parvus* from Bed 10B at the Pojue Section, the PTB of this section is placed at the uneven surface between Bed 10B (Early Triassic dolomitized mudstone) and Bed 10A (Late Permian cortoid foraminifera grainstone). This situation is closely similar to that of the GBG sections such as Dajiang where the PTB is placed at the uneven surface between Permian bioclastic packstone and Lower Triassic wackstone (Jiang et al., 2014), and Yangtze platform section like Gaohua (Wang et al., 2016) where the PTB is also placed at the uneven surface between the upper Permian limestone to lower Triassic microbialite. The cause of truncation has been debated with both intense ocean acidification (Payne et al., 2007) and emergence followed by karstification being proposed (Wignall et al., 2009). Lehrmann et al. (2015) concluded that the thickness for anisopachous fibrous cements below the truncation surface are random without a downward orientation which suggested the truncation surface have formed by submarine dissolution and it caused 30~100kyr hiatus during the *C. meishanensis, H. changxingensis* and *C. taylorae* zones at Meishan (21kyr Wu et al., 2013). However, their evidence was refuted by Kershaw et al. (2016) who favoured physical erosion as the cause of truncation. Given the shallow-water setting

243 of the Napo Platform sections, we consider it likely that a minor sequence boundary
244 due to regression is seen in the studied sections.

245 *H. parvus* is absent from Bed 9 at the Dala Section, but comparison with the nearby
246 Pojue section (only 37 km away) and considering the similar lithological sequence and
247 the fact that *H. praeparvus* was found at the base of dolomitized mudstone below the
248 microbialite, we surmise that the PTB is likely to occur at the base Bed 9 at Dala. Also,
249 as noted above, the Permian-Triassic boundary at Dajiang has also been placed at the
250 base of a wackstone below the microbialite, similar to Gaohua (Wang et al., 2016) and
251 Jianzishan (Bai et al., 2018) sections. This inference is supported by the similar negative
252 shifts seen in the $\delta^{13}C_{carb}$ curve at these two sections. The *Hindeodus changxingensis*
253 Zone is also probably missing in these two sections (cf. Jiang et al., 2014). This was
254 followed by the development of the dolomitized mudstone bed and subsequently the
255 microbialite bed during the *H. parvus* Zone. The first occurrence of *H. parvus* in some
256 microbialite sections lead Brosse et al. (2015) to argue that this species is an unreliable
257 marker for the base of the Triassic at the Meishan GSSP. In detail, they found that *H.*
258 *parvus* first appears below *H. eurypyge* and *I. turgida* in their microbialite-bearing study
259 section at Wuzhuan whereas *H. parvus* first appears above these species at Meishan
260 (Jiang et al., 2007). These observations lead Brosse et al. to conclude that *H. parvus*
261 appears “late” at Meishan. Alternatively, we note that both *H. eurypyge* and *I. turgida*
262 are very rare at Wuzhuan – the former species is only known from a single element –
263 indicating that they are unlikely to show a range comparable with that at Meishan. Both
264 these species are also rare conodonts in our samples from Dala and they are absented

from Pojue. Collection failure of *H. eurypyge* and *I. turgida* from microbialites is a more parsimonious interpretation of conodont distributions reported by Brosse et al. (2015).

5.2 Implications for the mass extinction

Shen et al. (2011) estimated that the mass extinction during the PTB lasted for almost 200 kyr and was accompanied by a negative C isotope excursion. This interval was revised down to about 60±48 kyr by Burgess et al. (2014), and shortened further to ~31±31 kyr at Penglaitan section (Shen et al., 2018). Song et al. (2013) demonstrated that there were two pulses of extinction straddling the PTB. Wang et al. (2014) attributed Song et al.'s finding to the Signor-Lipps effect and facies-dependent occurrences and concluded that there was a single extinction phase. However, Wang et al. (2014) failed to appreciate that the Song et al. study placed the second phase of extinction in the Early Triassic whereas the Signor-Lipps effect is only capable of making a mass extinction appear older not younger in time. In other words, implicit in the conclusion of Wang and colleagues is that the PTB mass extinction is an earliest Triassic event even though they favored a single, latest Permian extinction event. Jiang et al. (2015) reported an end-Permian foraminifera extinction at Bianyang, a deep-water location, which was later than that seen at Meishan. In contrast, He et al. (2015) suggested the deep-water brachiopods disappeared earlier than shallow-water brachiopods. Thus, extinction patterns clearly vary in different depositional settings in South China and span from the latest Permian to the earliest Triassic (see also Song et al., 2014). Biostratigraphically, the maximum extinction interval ranges from Bed 24e

to Bed 28 at Meishan (Shen et al., 2011) and thus started in the *C. meishanensis* Zone and ended in the *I. staeschei* Zone (Jiang et al., 2007, Chen Z.Q et al., 2015). Although the *H. changxingensis* Zone is likely absent at Dala and Pojue, these sections still record most of the PTB interval. It is interesting that the $\delta^{13}C_{carb}$ record at the two sections also shows lower values during the extinction interval (Fig. 7). This correspondence is also seen at the Dajiang section in GBG area (Luo et al., 2010) and at many other sections such as the Meishan GSSP (Shen et al., 2013; Fig. 7). Pojue and Dajiang sections both show a single negative shift beginning at the end of the Permian and culminating in an Earliest Triassic low of about 0 to -1‰, (Yin et al. 2014). Considering the *C. meishanensis* (±*H. changxingensis*) missing zone(s) (Yin et al., 2014), the shallow platform facies sections also can be correlated with the Meishan section through the $\delta^{13}C_{carb}$ excursion, despite only one negative excursion observed at shallow water sections. Pojue, Dala, and Dajiang (shallow water) sections have higher carbon isotope values in the extinction interval, of about 0 to -1‰, than deeper water sections like Meishan which have negative values of about -2 to -5‰ (Song et al., 2012).

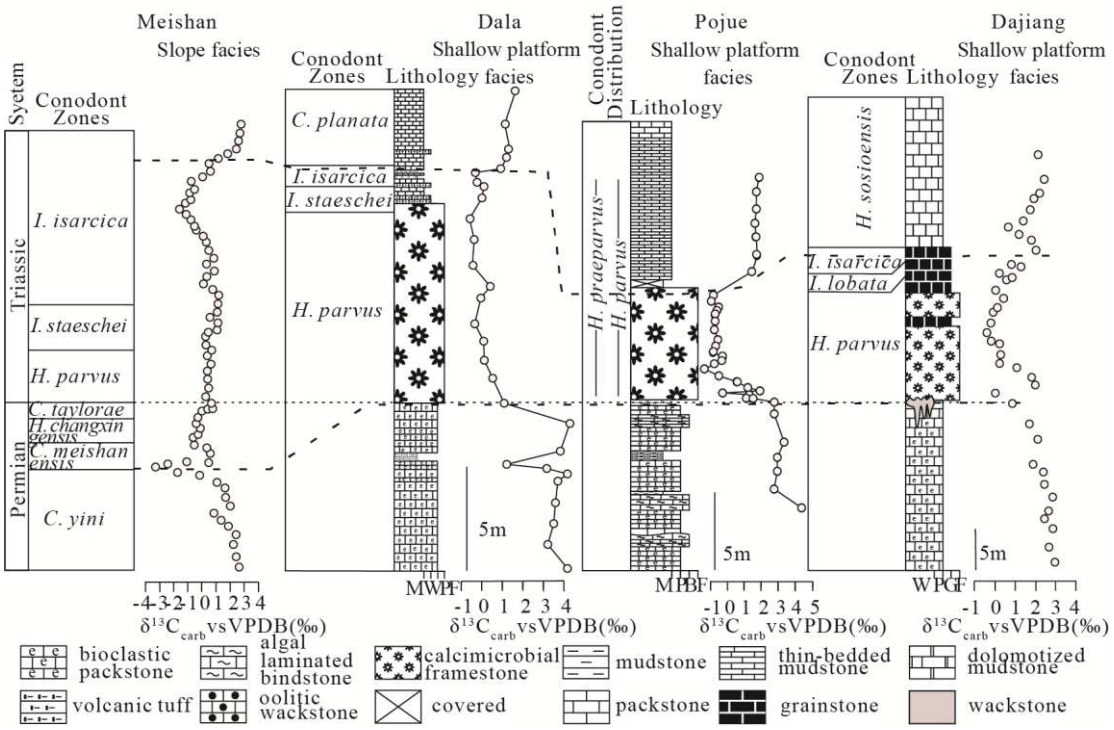

Figure. 7 Correlation of $\delta^{13}C_{carb}$ carbon curve and conodont zones for Pojue, Dala, Dajiang (Jiang et al., 2014; Luo et al.,2010), and Meishan GSSP (Shen et al., 2013). Abbreviations of the genus of conodont: *H. Hindeodus, C. Clarkina, I. Isarcicella.*

The Permian-Triassic mass extinction was not a sudden event in South China, but a phase of progressive environmental deterioration, spanning a few hundred thousand years, linked to rapid global warming and the widespread development of marine anoxia (e.g. Jiang et al., 2015; Song et al., 2014). The microbialites of the Napo Platform developed on carbonate platforms during the PTB extinction and represent a simple microbial ecosystem (Wang et al., 2011). The abundant microbes could have served as a major food source and also provided a local oxygen supply, thereby enhancing the hospitality of the ecosystem and providing a refuge for ostracods and other organisms, although the community lacked a well-developed trophic hierarchy (Forel et al., 2013). The organisms present in the microbialite ecosystems (bivalves,

316 ostracods and microgastropods) belong to groups with exceptional tolerance to high
317 temperatures (Song et al., 2014), a factor that may also have been important in their
318 occurrence. Unusually diverse bivalve and gastropod assemblages have also been
319 reported from the contemporary microbialites at the Shanggan section, Leye County,
320 Guangxi, South China (Hautmann et al., 2011). Thus, like deep-water settings,
321 microbialites offered a temporary refuge during the PTB mass extinction.
322

323 ## 6. Conclusions

324 The conodont biostratigraphy and carbon isotope record across the PTB at Pojue and
325 Dala on the Napo Platform have been documented. Four conodont zones: *H. parvus*
326 Zone, *I. staeschei* Zone, *I. isarcica* Zone and *C. planata* Zone are identified at Dala.
327 Defined by the first occurrence of *H. parvus,* the PTB is placed at the base of a
328 dolomitized bed (Bed 10 B) at Pojue. Correlating, using lithofacies development and
329 carbon isotope stratigraphy, the PTB at Dala is also placed at the base of a similar
330 dolomitized bed (base of Bed 9 Fig.5 B). The idea that *H. parvus* appears at a lower
331 level in microbialite sections than in the Meishan Stratotype are based on the late
332 occurrence of the rare species *H. eurypyge* and *I. turgida* in the microbialites and so we
333 suggest that this notion is unsafe.

334 Both carbon isotope curves at the two sections show lower values during the mass
335 extinction interval implying that the mass extinction was not a sudden event. The Napo
336 Platform sections show a sequence of events that provide much detail on the cause of
337 the mass extinction. Thus, latest Permian times saw the development of shallow-water

packstone facies with a high-diversity fauna. These strata are truncated and a hiatus spanning the *C. meishanensis* and *H. changxingensis* Zone is developed. The mass extinction began during this unrecorded interval on the Napo Platform.

Acknowledgements

This work was supported by the National Natural Science Foundation of China (grants no. 41572324), Special Project on Basic work of science and technology from National Ministry of Science and Technology of China (Sub-project, 2015FY310100-11 to HSJ) and the China Geological Survey (DD20160120-04 to HSJ). SEM pictures and carbon isotopes data were undertaken at the State Key Laboratory of Biogeology and Environmental Geology (China). We thank Suxin Zhang, Yuheng Fang for their assistance in SEM. Thanks also due to Huyue Song for the help in processing the carbon isotopes data.

References Cited

Bai, R.Y., Dai, X., Song, H.J., 2017, Conodont and Ammonoid Biostratigraphies around the Permian-Triassic boundary from Jianzishan of South China: Journal of Earth Science, 28(4): 595-613. https://doi.org/10.1007/s12583-017-0754-4

Baresel, B., Bucher, H., Bagherpour, B., et al., 2017. Timing of global regression and microbial bloom linked with the Permian-Triassic boundary mass extinction: implications for driving mechanisms. Scientific Reports, 7(1): 43630. https://doi.org/10.1038/srep43630

359 Baud, A., Richoz, S., Pruss, S., 2007. The lower Triassic anachronistic carbonate facies in space
360 and time. Global and Planetary Change, 55(1–3): 81-89.
361 https://doi.org/10.1016/j.gloplacha.2006.06.008
362 Baud, A., Richoz, S., Pruss, S., 2007. The Lower Triassic Anachronistic Carbonate Facies in Space
363 and Time. Global and Planetary Change, 55(1/2/3): 81–89.
364 https://doi.org/10.1016/j.gloplacha.2006.06.008
365 Brand, U., Blamey, N., Garbelli, C., et al., 2016. Methane Hydrate: Killer Cause of Earth's Greatest
366 Mass Extinction. Palaeoworld, 25(4): 496–507. https://doi.org/10.1016/j.palwor.2016.06.002
367 Brosse, M., Bucher, H., Bagherpour, B., et al., 2015. Conodonts from the Early Triassic Microbialite
368 of Guangxi (South China): Implications for the Definition of the Base of the Triassic System.
369 Palaeontology, 58(3): 563–584. https://doi.org/10.1111/pala.12162
370 Burgess, S. D., Bowring, S., Shen, S. Z., 2014. High-Precision Timeline for Earth's Most Severe
371 Extinction. Proceedings of the National Academy of Sciences, 111(9): 3316–3321.
372 https://doi.org/10.1073/pnas.1317692111
373 Chen, B., Joachimski, M. M., Wang, X. D., et al., 2016. Ice Volume and Paleoclimate History of
374 the Late Paleozoic Ice Age from Conodont Apatite Oxygen Isotopes from Naqing (Guizhou,
375 China). Palaeo- geography, Palaeoclimatology, Palaeoecology, 448: 151–161.
376 https://doi.org/10.1016/j.palaeo.2016.01.002
377 Chen, J., Beatty, T. W., Henderson, C. M., et al., 2009. Conodont Biostratigraphy across the
378 Permian-Triassic Boundary at the Dawen Section, Great Bank of Guizhou, Guizhou Province,
379 South China: Implications for the Late Permian Extinction and Correlation with Meishan.
380 Journal of Asian Baud, A., Richoz, S., Pruss, S., 2007. The Lower Triassic Anachronistic

Carbonate Facies in Space and Time. Global and Planetary Change, 55(1/2/3): 81–89. https://doi.org/10.1016/j.gloplacha.2006.06.008

Brand, U., Blamey, N., Garbelli, C., et al., 2016. Methane Hydrate: Killer Cause of Earth's Greatest Mass Extinction. Palaeoworld, 25(4): 496–507. https://doi.org/10.1016/j.palwor.2016.06.002

Brosse, M., Bucher, H., Bagherpour, B., et al., 2015. Conodonts from the Early Triassic Microbialite of Guangxi (South China): Implications for the Definition of the Base of the Triassic System. Palaeontology, 58(3): 563–584. https://doi.org/10.1111/pala.12162

Burgess, S. D., Bowring, S., Shen, S. Z., 2014. High-Precision Timeline for Earth's Most Severe Extinction. Proceedings of the National Academy of Sciences, 111(9): 3316–3321. https://doi.org/10.1073/pnas.1317692111

Chen, B., Joachimski, M. M., Wang, X. D., et al., 2016. Ice Volume and Paleoclimate History of the Late Paleozoic Ice Age from Conodont Apatite Oxygen Isotopes from Naqing (Guizhou, China). Palaeo- geography, Palaeoclimatology, Palaeoecology, 448: 151–161. https://doi.org/10.1016/j.palaeo.2016.01.002

Chen, B., Joachimski, M.M., Wang, X.D., et al., 2016. Ice volume and paleoclimate history of the Late Paleozoic Ice Age from conodont apatite oxygen isotopes from Naqing (Guizhou, China). Palaeogeography, Palaeoclimatology, Palaeoecology, 448: 151-161. https://doi.org/10.1016/j.palaeo.2016.01.002

Chen, J., Beatty, T. W., Henderson, C. M., et al., 2009. Conodont Biostratigraphy across the Permian-Triassic Boundary at the Dawen Section, Great Bank of Guizhou, Guizhou Province, South China: Implications for the Late Permian Extinction and Correlation with Meishan. Journal of Asian Earth Sciences, 36(6): 442–458. https://doi.org/10.1016/j.jseaes.2008.08.002

403 Clarkson, M.O., Kasemann, S.A., Wood, R.A., et al., 2015. Ocean acidification and the Permo-
404 Triassic mass extinction. Science, 348(6231): 229-232.
405 https://doi.org/10.1126/science.aaa0193
406 Chen, Z.-Q., Yang, H., Luo, M., et al., 2015. Complete Biotic and Sedimen- tary Records of the
407 Permian-Triassic Transition from Meishan Section, South China: Ecologically Assessing Mass
408 Extinction and Its After math. Earth-Science Reviews, 149: 67-107.
409 https://doi.org/10.1016/j.earscirev.2014.10.005
410 Clark, D. L., 1959. Conodonts from the Triassic of Nevada and Utah. Jour- nal of Paleontology,
411 33(2): 305–312
412 Clarkson, M. O., Kasemann, S. A., Wood, R. A., et al., 2015. Ocean Acidi- fication and the Permo-
413 Triassic Mass Extinction. Science, 348(6231): 229–232.
414 https://doi.org/10.1126/science.aaa0193
415 Ernst, R. E., Youbi, N., 2017. How Large Igneous Provinces Affect Global Cli- mate, sometimes
416 Cause Mass Extinctions, and Represent Natural Markers in the Geological Record.
417 Palaeogeography, Palaeoclimatology, Palaeoecol- ogy, 478: 30–52.
418 https://doi.org/10.1016/j.palaeo.2017.03.014
419 Ezaki, Y., Liu, J., Nagano, T., et al., 2008. Geobiological Aspects of the Earliest Triassic
420 Microbialites along the Southern Periphery of the Tropical Yangtze Platform: Initiation and
421 Cessation of a Microbial Regime. PALAIOS, 23(6): 356–369.
422 https://doi.org/10.2110/palo.2007.p07-035r
423 Forel, M. B., Crasquin, S., Kershaw, S., et al., 2013. In the Aftermath of the End-Permian Extinction:
424 The Microbialite Refuge?. Terra Nova, 25(2): 137–143. https://doi.org/10.1111/ter.12017

425 Foster, W. J., Danise, S., Price, G. D., et al., 2017. Subsequent Biotic Crises Delayed Marine
426 Recovery Following the Late Permian Mass Extinc- tion Event in Northern Italy. PLOS ONE,
427 12(3): e0172321. https://doi.org/10.1371/journal.pone.0172321
428 Grasby, S. E., Beauchamp, B., Knies, J., 2016. Early Triassic Productivity Crises Delayed Recovery
429 from World's Worst Mass Extinction. Geol- ogy, 44(9): 779–782.
430 https://doi.org/10.1130/g38141.1
431 Hautmann, M., Bucher, H., Brühwiler, T., et al., 2011. An Unusually Di- verse Mollusc Fauna from
432 the Earliest Triassic of South China and Its Implications for Benthic Recovery after the End-
433 Permian Biotic Crisis. Geobios, 44(1): 71–85. https://doi.org/10.1016/j.geobios.2010.07.004
434 He, W. H., Shi, G. R., Twitchett, R. J., et al., 2015. Late Permian Marine Ecosystem Collapse Began
435 in Deeper Waters: Evidence from Brachiopod Diversity and Body Size Changes. Geobiology,
436 13(2): 123–138. https://doi.org/10.1111/gbi.12119
437 Huckriede, R., 1958. Die Conodonten Der Mediterranen Trias und Ihr Stratigraphischer Wert.
438 Paläontologische Zeitschrift, 32(3/4): 141–175
439 Jiang, H. S., Aldridge, R. J., Lai, X. L., et al., 2011. Phylogeny of the Conodont Genera Hindeodus
440 and Isarcicella across the Permian-Triassic Boundary. Lethaia, 44(4): 374–382.
441 https://doi.org/10.1111/j.1502-3931.2010.00248.x
442 Jiang, H. S., Joachimski, M. M., Wignall, P. B., et al., 2015. A Delayed End-Permian Extinction in
443 Deep-Water Locations and Its Relationship to Temperature Trends (Bianyang, Guizhou
444 Province, South China). Palaeogeography, Palaeoclimatology, Palaeoecology, 440: 690–695.
445 https://doi.org/10.1016/j.palaeo.2015.10.002

446 Jiang, H. S., Lai, X. L., Luo, G. M., et al., 2007. Restudy of Conodont Zonation and Evolution
447 across the P/T Boundary at Meishan Section, Changxing, Zhejiang, China. Global and
448 Planetary Change, 55(1/2/3): 39–55. https://doi.org/10.1016/j.gloplacha.2006.06.007
449 Jiang, H. S., Lai, X. L., Sun, Y. D., et al., 2014. Permian-Triassic Conodonts from Dajiang (Guizhou,
450 South China) and Their Implication for the Age of Microbialite Deposition in the Aftermath
451 of the End-Permian Mass Extinction. Journal of Earth Science, 25(3): 413–430.
452 https://doi.org/10.1007/s12583-014-0444-4
453 Joachimski, M. M., Lai, X., Shen, S., et al., 2012. Climate Warming in the Latest Permian and the
454 Permian-Triassic Mass Extinction. Geology, 40(3): 195–198.
455 https://doi.org/10.1130/g32707.1
456 Kershaw, S., Collin, P. Y., Crasquin, S., 2016. Comment to Lehrmann et al. New Sections and
457 Observations from the Nanpanjiang Basin, South China. PALAIOS, 31(3): 111–117.
458 https://doi.org/10.2110/palo.2015.093
459 Kozur, H., 1995. Some Remarks to the Conodonts Hindeodus and Isar- cicella in the Latest Permian
460 and Earliest Triassic. Palaeoworld, 6: 64–77
461 Kozur, H., 1996. The Conodonts Hindeodus, Isarcicella, Sweetohindeodus in the Uppermost
462 Permian and Lowermost Triassic. Geologia Croatica, 49(1): 81–116
463 Kozur, H., Mostler, H., Rahimi-Yazd, A., 1975. Beiträge zur Mikrofauna Permotriadischer
464 Schichtfolgen Teil II: Neue Conodonten aus dem Oberperm und der Basalen Trias von Nord-
465 und Zentraliran. Geol. Palaont. Mitt. Innsbruck, 5(3): 1–23

466 Kozur, H., Pjatakova, M., 1976. Die Conodontenart Anchignathodus parvus n.sp., eine wichtige
467 Leiform der basalen Trias. Proceedings Koninkl Nederland Akademie van Wetenschappen,
468 Series B, 79: 123–128
469 Krull, E. S., Lehrmann, D. J., Druke, D., et al., 2004. Stable Carbon Isotope Stratigraphy across the
470 Permian-Triassic Boundary in Shallow Marine Carbonate Platforms, Nanpanjiang Basin,
471 South China. Palaeo- geography, Palaeoclimatology, Palaeoecology, 204(3/4): 297–315.
472 https://doi.org/10.1016/s0031-0182(03)00732-6
473 Lehrmann, D. J., Bentz, J. M., Wood, T., et al., 2015. Environmental Con- trols on the Genesis of
474 Marine Microbialites and Dissolution Surface Associated with the End-Permian Mass
475 Extinction: New Sections and Observations from the Nanpanjiang Basin, South China.
476 PALAIOS, 30(7): 529–552. https://doi.org/10.2110/palo.2014.088
477 Lehrmann, D. J., Minzoni, M., Li, X. W., et al., 2012. Lower Triassic Oolites of the Nanpanjiang
478 Basin, South China: Facies Architecture, Giant Ooids, and Diagenesis—Implications for
479 Hydrocarbon Reservoirs. AAPG Bulletin, 96(8): 1389–1414.
480 https://doi.org/10.1306/01231211148
481 Lehrmann, D. J., Payne, J. L., Felix, S. V., et al., 2003. Permian-Triassic Bound- ary Sections from
482 Shallow-Marine Carbonate Platforms of the Nanpanjiang Basin, South China: Implications for
483 Oceanic Conditions Associated with the End-Permian Extinction and Its Aftermath.
484 PALAIOS, 18(2): 138–152. https://doi.org/10.1669/0883-1351(2003)18<138:pbsfsc>2.0.co;2
485 Li, F., Yan, J. X., Algeo, T., et al., 2013. Paleoceanographic Conditions Following the End-Permian
486 Mass Extinction Recorded by Giant Ooids (Moyang, South China). Global and Planetary
487 Change, 105: 102–120. https://doi.org/10.1016/j.gloplacha.2011.09.009

488 Li, F., Yan, J. X., Chen, Z. Q., et al., 2015. Global Oolite Deposits Across the Permian-Triassic
489 Boundary: A Synthesis and Implications for Palaeocean- ography Immediately after the End-
490 Permian Biocrisis. Earth-Science Re- views, 149: 163–180.
491 https://doi.org/10.1016/j.earscirev.2014.12.006
492 Li, Z. S., Zhan L. P., Dai, J. Y., et al., 1989. Study on the Permian-Triassic Biostratigraphy and
493 Event Stratigraphy of Northern Sichuan and Southern Shaanxi. Geological Memoirs Vol. 9.
494 Geological Publishing House, Beijing. 448 (in Chinese)
495 Liu, J. B., Ezaki, Y., Yang, S. R., et al., 2007. Age and Sedimentology of Microbialites after the
496 End-Permian Mass Extinction in Luodian, Guizhou Province. Journal of Palaeogeography,
497 9(5): 473–486 (in Chinese with English Abstract)
498 Luo, G. M., Kump, L. R., Wang, Y. B., et al., 2010. Isotopic Evidence for an Anomalously Low
499 Oceanic Sulfate Concentration Following End-Permian Mass Extinction. Earth and Planetary
500 Science Letters, 300(1/2): 101–111. https://doi.org/10.1016/j.epsl.2010.09.041
501 Nicoll, R. S., Metcalfe, I., Wang, C. Y., 2002. New Species of the Conodont Genus Hindeodus and
502 the Conodont Biostratigraphy of the Per- mian-Triassic Boundary Interval. Journal of Asian
503 Earth Sciences, 20(6): 609–631. https://doi.org/10.1016/s1367-9120(02)00021-4
504 Orchard, M. J., Nassichuk, W. W., Rui, L., 1994. Conodonts from the Lower Griesbachian Otoceras
505 Latilobatum Bed of Selong, Tibet and the Posi tion of the Permian-Triassic boundary. Memoir-
506 Canadian Society of Petroleum Geologists, 17: 823–843
507 Payne, J. L., Lehrmann, D. J., Follett, D., et al., 2007. Erosional Truncation of Uppermost Permian
508 Shallow-Marine Carbonates and Implications for Permian-Triassic Boundary Events.
509 Geological Society of America Bulletin, 119(7/8): 771–784. https://doi.org/10.1130/b26091.1

510 Perri, M. C., Farabegoli, F., 2003. Conodonts across the Permian-Triassic Boundary in the Southern
511 Alps. In: Mawson, R., Talent, J. A., eds., Contributions to the Second Australian Conodont
512 Symposium. Courier Forschungsinstitut Senckenberg Series, 281–313
513
514 Regional Geological Survey Team of the Guangxi Zhuang Autonomous Region Geological Bureau,
515 1974. 1 : 20 000 Regional Geological Sur- vey Report of the People's Republic of China: Baise
516 Map and Delong Map, Geological Part. Guangxi Zhuang Autonomous Region Geologi- cal
517 Bureau, Yishan. 1–188 (in Chinese)
518 Shen, S. Z., Cao, C. Q., Zhang, H., et al., 2013. High-Resolution δ13Ccarb Chemostratigraphy from
519 Latest Guadalupian through Earliest Triassic in South China and Iran. Earth and Planetary
520 Science Letters, 375: 156–165. https://doi.org/10.1016/j.epsl.2013.05.020
521 Shen, S. Z., Crowley, J. L., Wang, Y., et al., 2011. Calibrating the End-Permian Mass Extinction.
522 Science, 334(6061): 1367–1372. https://doi.org/10.1126/science.1213454
523 Shen, S. Z., Ramezani, J., Chen, J., et al., 2018. A Sudden End-Permian Mass Extinction in South
524 China. GSA Bulletin. https://doi.org/ 10.1130/b31909.1
525 Song, H. J., Tong, J. N., Xiong, Y. L., et al., 2012. The Large Increase of δ13Ccarb-Depth Gradient
526 and the End-Permian Mass Extinction. Science China Earth Sciences, 55(7): 1101–1109.
527 https://doi.org/10.1007/ s11430-012-4416-1
528 Song, H. J., Wignall, P. B., Chu, D. L., et al., 2014. Anoxia/High Temperature Double Whammy
529 during the Permian-Triassic Marine Crisis and Its After- math. Scientific Reports, 4(1): 4132.
530 https://doi.org/10.1038/srep04132

Song, H. J., Wignall, P. B., Tong, J. N., et al., 2013. Two Pulses of Extinc- tion during the Permian-Triassic Crisis. Nature Geoscience, 6(1): 52–56. https://doi.org/10.1038/ngeo1649

Sun, H., Xiao, Y. L., Gao, Y. J., et al., 2018. Rapid Enhancement of Chemical Weathering Recorded by Extremely Light Seawater Lithium Isotopes at the Permian-Triassic Boundary. Proceedings of the National Academy of Sci- ences, 115(15): 3782–3787. https://doi.org/10.1073/pnas.1711862115

Sun, Y. D., Joachimski, M. M., Wignall, P. B., et al., 2012. Lethally Hot Temperatures during the Early Triassic Greenhouse. Science, 338(6105): 366–370. https://doi.org/10.1126/science.1224126

Tian, L., Bottjer, D. J., Tong, J. N., et al., 2015. Distribution and Size Varia- tion of Ooids in the Aftermath of the Permian-Triassic Mass Extinction. PALAIOS, 30(9): 714–727. https://doi.org/10.2110/palo.2014.110

Wang, C. Y., 1996. Conodont Evolutionary Lineage and Zonation for the Latest Permian and the Earliest Triassic. Permophiles, 29: 30–37

Wang, L. N., Wignall, P. B., Wang, Y. B., et al., 2016. Depositional Condi- tions and Revised Age of the Permo-Triassic Microbialites at Gaohua Section, Cili County (Hunan Province, South China). Palaeogeography, Palaeoclimatology, Palaeoecology, 443: 156–166. https://doi.org/10.1016/j.palaeo.2015.11.032

Wang, Y., Sadler, P. M., Shen, S. Z., et al., 2014. Quantifying the Process and Abruptness of the End-Permian Mass Extinction. Paleobiology, 40(1): 113–129. https://doi.org/10.1666/13022

551 Wignall, P. B., 2015. The Worst of Times: How Life on Earth Survived Eighty Million Years of
552 Extinctions. Princeton University Press, Princeton. 224.
553 https://doi.org/10.1515/9781400874248
554 Wignall, P. B., Hallam, A., 1996. Facies Change and the End-Permian Mass Extinction in S.E.
555 Sichuan, China. PALAIOS, 11(6): 587–596. https://doi.org/10.2307/3515193
556 Wignall, P. B., Kershaw, S., Collin, P. Y., et al., 2009. Erosional Truncation of Uppermost Permian
557 Shallow-Marine Carbonates and Implications for Permian-Triassic Boundary Events:
558 Comment. Geological Society of America Bulletin, 121(5/6): 954–956.
559 https://doi.org/10.1130/b26424.1
560 Wu, H. C., Zhang, S. H., Hinnov, L. A., et al., 2013. Time-Calibrated Mi- lankovitch Cycles for the
561 Late Permian. Nature Communications, 4(1): 2452. https://doi.org/10.1038/ncomms3452
562 Xiang, L., Schoepfer, S. D., Zhang, H., et al., 2016. Oceanic Redox Evolu- tion across the End-
563 Permian Mass Extinction at Shangsi, South China. Palaeogeography, Palaeoclimatology,
564 Palaeoecology, 448: 59–71. https://doi.org/10.1016/j.palaeo.2015.10.046
565 Yan, C. B., Wang, L. N., Jiang, H. S., et al., 2013. Uppermost Permian to Lower Triassic Conodonts
566 at Bianyang Section, Guihzou Province, South China. PALAIOS, 28(8): 509–522.
567 https://doi.org/10.2110/palo.2012.p12-077r
568 Yang, B., Lai, X. L., Wignall, P. B., et al., 2012. A Newly Discovered Ear- liest Triassic Chert at
569 Gaimao Section, Guizhou, Southwestern China. Palaeogeography, Palaeoclimatology,
570 Palaeoecology, 344/345: 69–77. https://doi.org/10.1016/j.palaeo.2012.05.019

571 Yin, H. F., Jiang, H. S., Xia, W. C., et al., 2014. The End-Permian Regression in South China and
572 Its Implication on Mass Extinction. Earth-Science Reviews, 137: 19–33.
573 https://doi.org/10.1016/j.earscirev.2013.06.003
574 Yin, H. F., Xie, S. C., Luo, G. M., et al., 2012. Two Episodes of Environ- mental Change at the
575 Permian-Triassic Boundary of the GSSP Section Meishan. Earth-Science Reviews, 115(3):
576 163–172. https://doi.org/ 10.1016/j.earscirev.2012.08.006
577 Yin, H. F., Zhang, K. X., Tong, J. N., et al., 2001. The Global Stratotype Section and Point (GSSP)
578 of the Permian-Triassic Boundary. Episodes, 24(2): 102–114
579 Yuan, J. L., Jiang, H. S., Wang, D. C., 2015. LST: A New Inorganic Heavy Liquid Used in Conodont
580 Separation. Geological Science and Tech- nology Information, 34(5): 6 (in Chinese with
581 English Abstract)
582 Zhang, K. X., Tong, J. N., Lai, X. L., et al., 2009. Progress on Study of Conodont Sequence for the
583 GSSP Section at Meishan, Changxing, Zhejiang Province, South China. Acta Palaeontologica
584 Sinica, 48(3): 474–486 (in Chinese with English Abstract)
585 Zhang, N., Jiang, H. S., Zhong, W. L., et al., 2014. Conodont Biostratigra- phy across the Permian-
586 Triassic Boundary at the Xinmin Section, Guizhou, South China. Journal of Earth Science,
587 25(5): 779–786. https://doi.org/10.1007/s12583-014-0472-0
588 Zhao, X. M., Tong, J. N., Yao, H. Z., et al., 2008. Anachronistic Facies in the Lower Triassic of
589 South China and Their Implications to the Ecosys- tems during the Recovery Time. Science in
590 China Series D: Earth Sci- ences, 51(11): 1646–1657. https://doi.org/10.1007/s11430-008-
591 0128-y
592

Plates

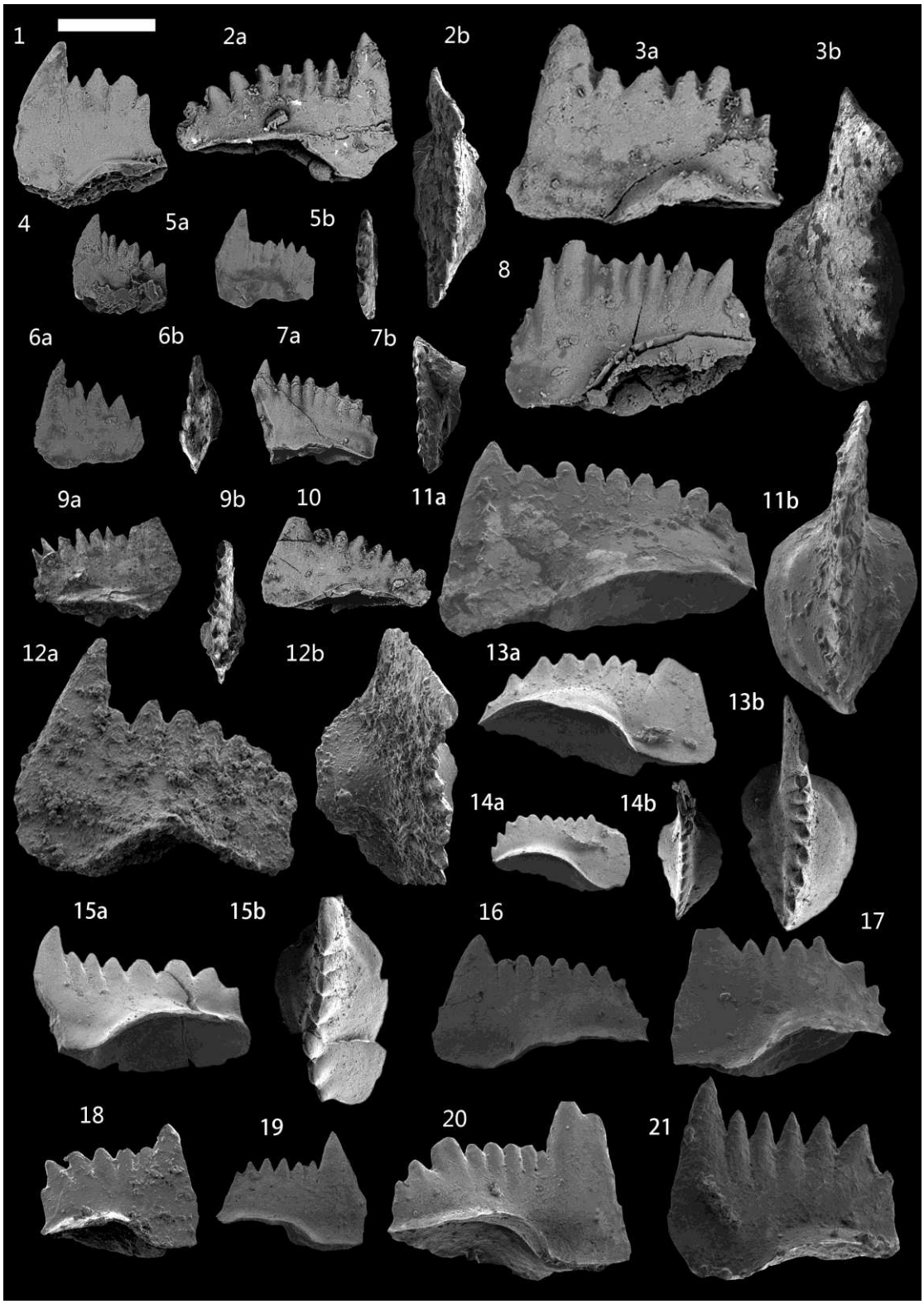

Plate.1 P_1 elements from Pojue and Dala sections. Scale bar equals 200μm. 1-11, obtained from Pojue section. 1,3,5,9. *Hindeodus parvus* (Kozur and Pjatakova, 1976); 1. Bed 10b, PJC-09, lateral view; 3. Bed 10b, PJC-09,

lateral view and upper view; 5. Bed 13, PJC-15, lateral view and upper view; 9. Bed 10b, PJC-09, lateral view and upper view. 2,4,6,7,8,10,11. *Hindeous praeparvus* Kozur,1996; 2. Bed 10c, PJC-10, lateral view and upper view; 4. Bed 13, PJC-14, lateral view; 6. Bed 10b, PJC-09, lateral view and upper view; 7. Bed 13, PJC-13, lateral view and upper view; 8; Bed 13, PJC-16, lateral view; 10. Bed 10c, PJC-10, lateral view; 11. Bed 10b, PJC-09, lateral view and upper view. 12-21, obtained from Dala section. 12,19,20. *Hindeodus parvus* (Kozur and Pjatakova,1976); 12. Bed 15, DAL-14, lateral view and upper view; 19. Bed 17, DAL-16, lateral view; 20. Bed 15, DAL-14, lateral view.13,14,15,16,18, 21. *Hindeodus praeparvus* Kozur,1996; 13,14,15. Bed 9, DAL-2B, lateral view and upper view; 16. Bed 17, DAL-15, lateral view; 18, 21. Bed 17, DAL-16, lateral view. 17. *Hindeodus inflatus* Nicoll et al., 2002; Bed 17, DAL-15, lateral view.

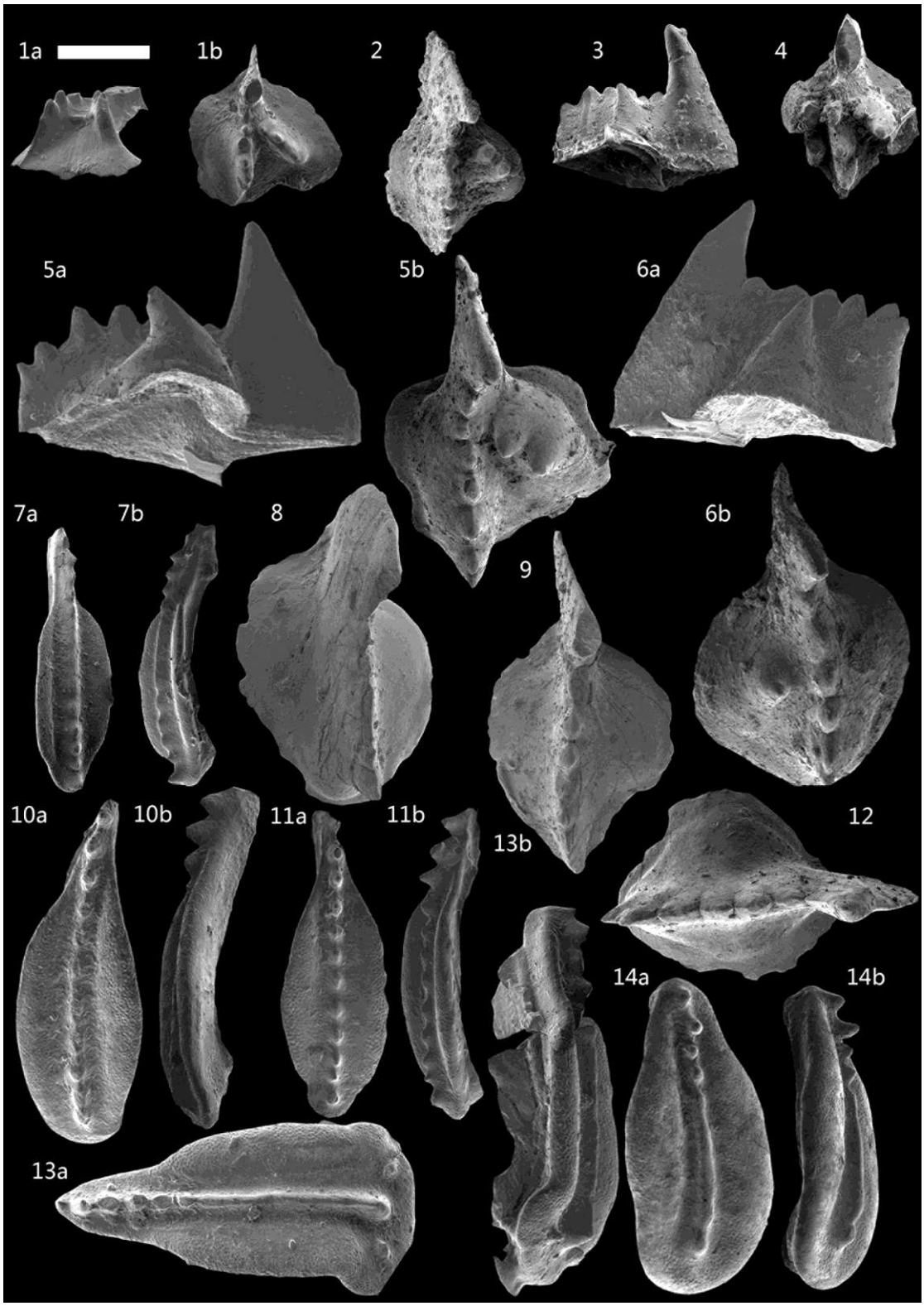

Plate. 2 P_1 elements from the Dala section. Scale bar equals 200μm. 1,2,3,5,6. *Isarcicella staeschei* Dai and Zhang, 1989; Bed 17, DAL-15, 1. lateral view and upper view; 2. upper view; 3. lateral view; 5,6. lateral view and upper view. 4. *Isarcicella isarcica* (Huckriede, 1958); Bed 12, DAL-13, upper view. 7. *Clarkina* cf. *carinata*; Bed 17,

610 DAL-15, lateral view and upper view. 8,9,12. *Isarcicella inflata* Perri and Farabegoli, 2003; Bed 15, DAL-14, upper

611 view. 10. *Clarkina lehrmanni* Chen et al., 2009; Bed 17, DAL-15, lateral view and upper view. 11. *Clarkina carinata*

612 (Clark, 1959); Bed 17, DAL-15, lateral view and upper view. 13. *Clarkina* sp.; Bed 17, DAL-15, lateral view and

613 upper view. 14. *Clarkina planata* (Clark, 1959); Bed 17, DAL-15, lateral view and upper view.

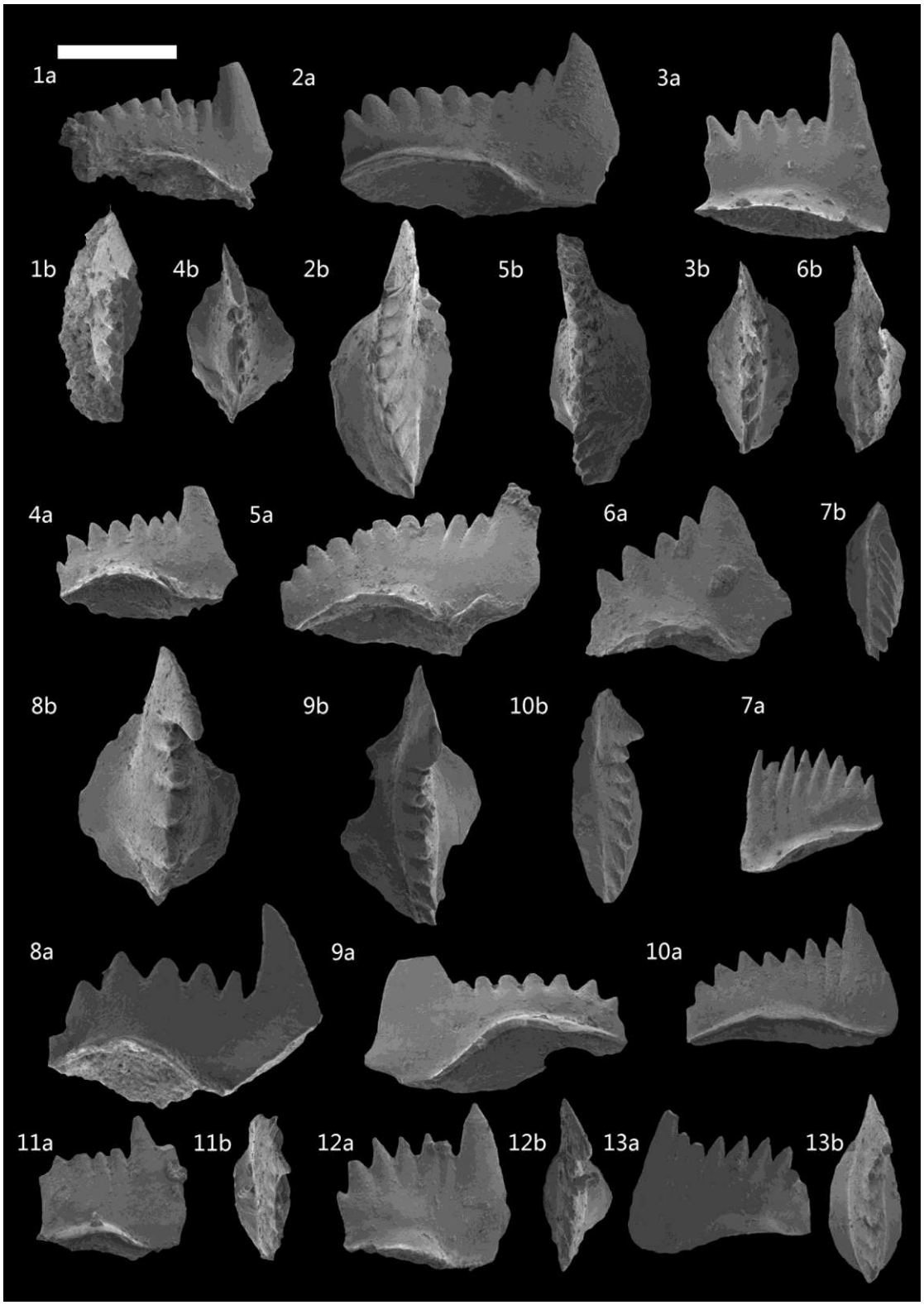

614

615 **Plate.3** P_1 elements from the Dala section. Scale bar equals 200μm. 1. *Hindeodus* cf. *parvus*; Bed 10, DAL-6, lateral

616 view and upper view. 2,4,5,6,7,10. *Hindeodus praeparvus* Kozur,1996; lateral view and upper view; 2. Bed 10, DAL-

617 6; 4,5. Bed 11, DAL-11; 6,7. Bed 11, DAL-12; 10. Bed 12, DAL-15. 3,11,12. *Hindeodus parvus* (Kozur and

Pjatakova, 1976); lateral view and upper view; 3. Bed 11, DAL-11; 11. Bed 11, DAL-12; 12. Bed 17, DAL-15. 8,9. *Isarcicella turgida* (Kozur et al., 1975); lateral view and upper view; 8. Bed 11, DAL-12; 9. Bed 17, DAL-15. 13. *Isarcicella prisca* Kozur, 1995; lateral view and upper view; Bed 17, DAL-15.

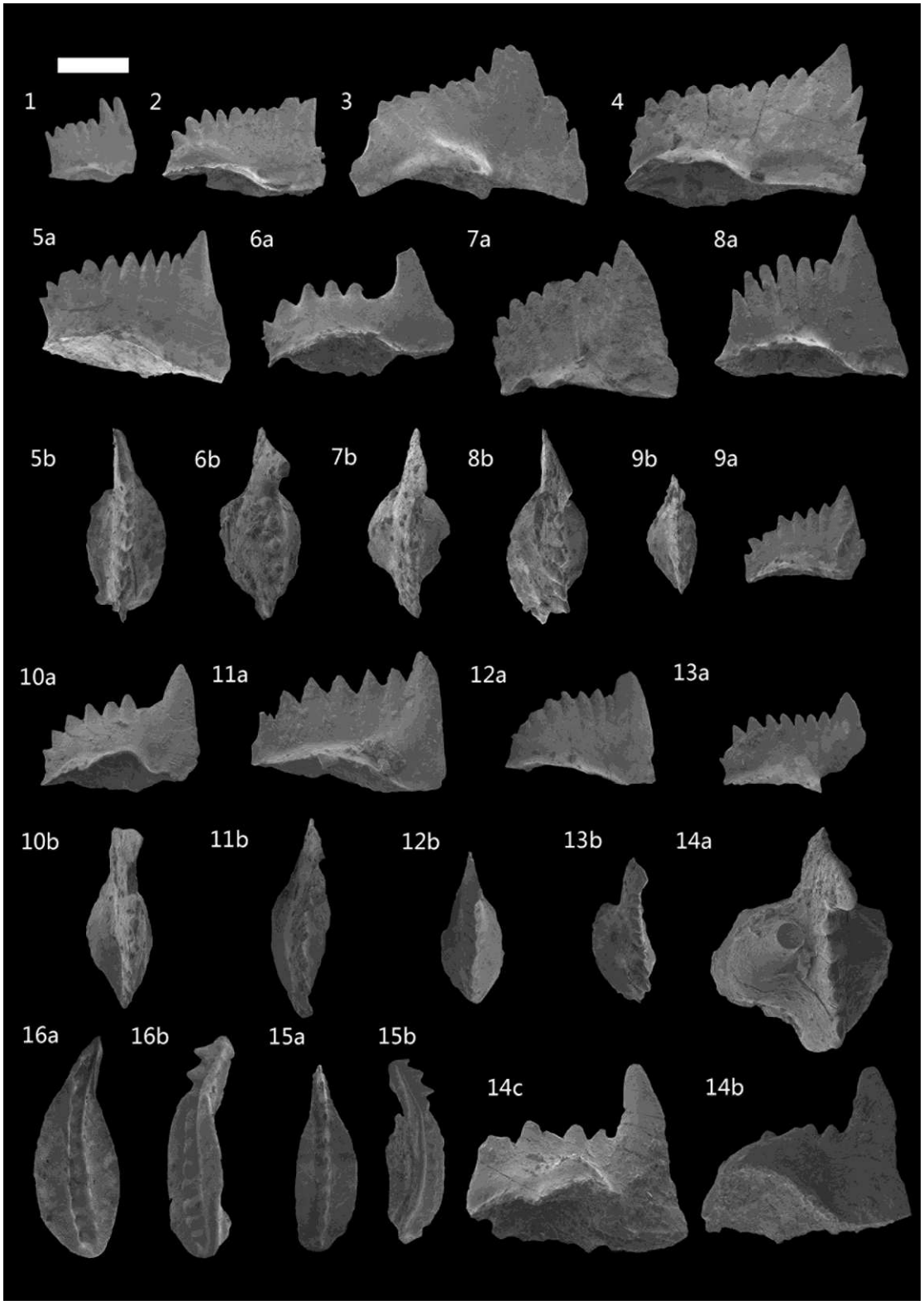

Plate. 4 P_1 elements from the Dala section. Scale bar equals 200μm.1,4,8,13. *Hindeodus parvus* (Kozur and Pjatakova, 1976); 1,4. Bed 17, DAL-15, lateral view; 8. Bed 17, DAL-17, lateral view and upper view; 13. Bed 17, DAL-18, lateral view and upper view. 2,3. *Hindeodus peculiaris* (Perri and Farabegoli, 2003); Bed 17, DAL-15, lateral view. 5,7,9,10,11,12. *Hindeodus praeparvus* Kozur,1996; 5,7,9. Bed 17, DAL-17, lateral view and upper view; 10,11,12. Bed 17, DAL-18, lateral view and upper view. 6. *Isarcicella turgida* (Kozur et al., 1975); Bed 17, DAL-15, upper view and lateral view. 14. *Isarcicella staeschei* Dai and Zhang, 1989; Bed 17, DAL-15, upper view and lateral view. 15.*Clarkina taylorae* (Orchard et al., 1994); Bed 17, DAL-15, upper view and lateral view. 16.*Clarkina lehrmanni* Chen et al., 2009; Bed 17, DAL-15, upper view and lateral view.